Preface

An *Integrated District Energy Assessment by Simulation* (IDEAS) tool is developed and allows integrated transient simulation of thermal and electrical processes at neighborhood level. The IDEAS tool differs from existing building physics and systems based and electrical energy system based models by (i) integrating the dynamics of the hydronic, thermal as well as electrical energy networks at (ii) both the building and aggregated level within a single model and solver.

The present document contains the complete specifications of the IDEAS tool. All equations are written in such way that positive energy flows increase the energy of the specific system. Unless stated differently, all variables are measured in SI units, i.e. length in meter and mass in kilogram. An exception is made for temperature where T depicts the absolute temperature in Kelvin and ϑ in degrees Celcius.

Leuven,   *Ruben Baetens*
January 2012   *Roel De Coninck*
                                                                              Juan Van Roy
                                                                          Bart Verbruggen

Contents

Part II   Validation or verification

Ruben Baetens and Dirk Saelens

Roel De Coninck and Lieve Helsen

Juan Van Roy, Bart Verbruggen and Johan Driesen

Part III   Bibliography

List of Contributors

Ruben Baetens
K.U.Leuven, Kasteelpark Arenberg 40 bus 2447, BE-3001 Leuven (Heverlee) e-mail:
ruben.baetens@bwk.kuleuven.be

Roel De Coninck
K.U.Leuven, Celestijnenlaan 300a bus 2421, BE-3001 Leuven (Heverlee) e-mail:
roel.deconinck@mech.kuleuven.be

Juan Van Roy
K.U.Leuven, Kasteelpark Arenberg 10 bus 2445, BE-3001 Leuven (Heverlee) e-mail:
juan.vanroy@esat.kuleuven.be

Bart Verbruggen
K.U.Leuven, Kasteelpark Arenberg 10 bus 2445, BE-3001 Leuven (Heverlee) e-mail:
bart.verbruggen@esat.kuleuven.be

Johan Driesen
K.U.Leuven, Kasteelpark Arenberg 10 bus 2445, BE-3001 Leuven (Heverlee) e-mail:
johan.driesen@esat.kuleuven.be

Lieve Helsen
K.U.Leuven, Celestijnenlaan 300a bus 2421, BE-3001 Leuven (Heverlee) e-mail:
lieve.helsen@mech.kuleuven.be

Dirk Saelens
K.U.Leuven, Kasteelpark Arenberg 40 bus 2447, BE-3001 Leuven (Heverlee) e-mail:
dirk.saelens@bwk.kuleuven.be

Part I
Specifications

spec-i-fi-ca-tion (n.) 1. the act of specifying. 2. a. specifications, A detailed, exact statement of particulars, especially a statement prescribing materials, dimensions, and quality of work for something to be built, installed, or manufactured. b. A single item or article that has been specified. 3. An exact written description of an invention by an applicant for a patent.

Chapter 1
Climate

Ruben Baetens and Dirk Saelens

Abstract A numeric building model is developed in Modelica for integrated energy simulation.

In this section, we describe in detail the climate model and its possibilities that are implemented in Modelica as part of the IDEAS platform. Four external factors are to be known, i.e. external temperature and ground temperature for transient heat losses by conduction, sky temperature for long-wave radiation losses and short-wave gains on surfaces by solar irradiation.

1.1 Weather data

The main weather parameters required for transient thermal building simulation are the ambient dry-bulb temperature $T_{db}(t)$, the outdoor relative humidity $\varphi_e(t)$, the wind speed $v_{10}(t)$, the diffuse horizontal solar radiation $E_{d,h}(t)$ and direct normal solar radiation $E_{D,\perp}(t)$.

The Meteonorm system [1] is a comprehensive source of (all mentioned) weather data for engineering applications in Europe and this system is used within this context. For simulation, the retrieved data from the Meteonorm system are not used within the common formats of a test reference year `*.try` [2, 3] as used in Europe or the formats of a typical meteorological years `*.tmy` or `*.tmy2` [4, **?**] and weather years for energy calculations `*.wyec` or `*.wyec2` [5] as used in the United States and Canada. These data formats are derived from hourly observations at a specific location by the national weather service or meteoro-

Ruben Baetens

KU Leuven, Kasteelpark Arenberg 40 bus 2447, BE-3001 Leuven (Heverlee) e-mail: ruben.baetens@ bwk.kuleuven.be

Dirk Saelens

KU Leuven, Kasteelpark Arenberg 40 bus 2447, BE-3001 Leuven (Heverlee) e-mail: dirk.saelens@ bwk.kuleuven.be

logical office and contain too little information for sub-hourly simulation, especially towards renewable energy generation by solar radiation.

From the retrieved data from the Meteonorm system, one more temperature needs to be determined. The long-wave radiative heat exchange of an exterior surface with a cloudy sky is calculated based on a sky temperature. This black-body sky temperature $T_{sky}(t)$ can be determined [6, 7] as

$$T_{sky}(t) = T_{db}(t)\varepsilon_{sky}(t)^{0.25} \tag{1.1}$$

$$\varepsilon_{sky}(t) = \varepsilon_0(t) + \Delta\varepsilon_h(t) + CCF(t)\left[1 - \varepsilon_h(t) - \Delta\varepsilon_h(t)\right] \tag{1.2}$$

where $\varepsilon_{sky}(t)$ is the cloudy sky emissivity [8, 9, 7], where $\varepsilon_0(t) + \Delta\varepsilon_h(t)$ is the clear sky emisivity $\varepsilon_{clear}(t)$, $\Delta\varepsilon_h(t)$ is a diurnal correction taking into account the difference in sky emissivity between day and night and $CCF(t)$ is the cloud cover factor. Both $\varepsilon_{clear}(t)$ and $CCF(t)$ are determined as polynomial fits on measurement data:

$$\varepsilon_0(t) + \Delta\varepsilon_h(t) = 0.711 + 0.0056\ \vartheta_{dew}(t) + 0.000073\ \vartheta_{dew}(t)^2 + 0.013\ \cos h(t) \tag{1.3}$$

$$CCF(t) = 1.0 + 0.024\ CC(t) - 0.0035\ CC(t)^2 + 0.00028\ CC(t)^3 \tag{1.4}$$

where $h(t)$ is the hour angle, $\vartheta_{dew}(t)$ is the dew temperature and $CC(t)$ is the tenths cloud cover retrieved from Meteonorm [10, 11].

1.2 Solar radiation

The calculation of the direct and diffuse solar irradiation on a tilted surface requires determination of the position of the sun in the sky. Here, the zenith angle $\xi(t,x)$ of surface with inclination $i(x)$ and azimuth $a(x)$ are able to uniquely define the the solar radiation on a tilted surface based on the determination of the annual and daily solar cycle by means of solar time and declination.

Within the computational model, all solar irradiation calculations are handled in `Commons.Meteo.Solar.RadSol` which is built-in in each surface receiving solar radiation.

1.2.1 Solar geometry

The *apparent solar time* $t_{sol}(t)$ expressed in seconds is based on daily apparent motion of the sun as seen from the earth. Solar noon is defined as the moment when the sun reaches the highest point in the sky. Solar time defined as

$$t_{sol}(t) = t_{std}(t) + 720\pi^{-1}\left[L_{std} - L_{loc}\right] + E_t(t) \tag{1.5}$$

$$E_t(t) = -120\,e\sin M(t) + 60\tan^2\left(\varepsilon/2\right)\sin\left(2M(t) + 2\lambda_p\right) \qquad (1.6)$$

where $t_{std}(t)$ is the standard time of the time zone, L_{std} is the reference meridian, L_{loc} is the lcoal meridian and E_t is the *equation of time* defining the difference between solar noon and noon of local civil time, $M(t)$ is the mean anomaly relating to the position of the sun to the earth in a Kepler orbit, ε is the earth obliquity and λ_p the ecliptic longitude of the periapsis, i.e. the closest approach of the earth to the sun.

Daylight saving time is taken into account within the simulation and corrects $t_{std}(t)$. Daylight saving time starts in the *European Economic Community* on March $31 - [(5y)/4 + 4]$ mod 7 and ends on October $31 - [(5y)/4 + 1]$ mod 7 where y denotes the year and mod denotes the remainder by division [12].

Before the zenith angle can be calculated, the declination δ and solar hour angle $h(t)$ is to be defined to fully specify the position of the sun as seen by an observer at a given time. Here, $\delta(t)$ depicts the angle between the solar beam and the equatorial plane, defined [13] as

$$\sin\delta(t) = \sin\varepsilon\cos\left(2\pi\left(n(t) + 10\right)n_y^{-1}\right) \qquad (1.7)$$

where ε is the earth obliquity, $n(t)$ is the one-based day number, i.e. 1 for January 1, and n_y is the length in days of the earth revolution equal to 365.25 days. The correction of 10 days is required as winter solstice, i.e. when the apparent position of the sun in the sky as viewed from the Earth reaches its most northern extreme, occurs at December 21.

The hour angle $h(t)$ depicts the angle between between the half plane of the Earth's axis and the zenith and the half plane of the Earth's axis and the given location, defined as

$$h(t) = 2\pi t_{sol}(t)\,86400^{-1} - \pi \qquad (1.8)$$

where $t_{sol}(t)$ is solar time.

Based on $\delta(t)$ and $h(t)$, the zenith angle $\xi(t,x)$ of a surface with inclination $i(x)$ and azimuth $a(x)$ can be uniquely defined. The zenith angle of the sun to a surface is the angle between this surface normal and the sun's beam, and is derived from [14, 15]

$$\begin{aligned}
\cos\xi(t,x) = {}& \sin\delta(t)\sin\varphi\cos i(x) - \sin\delta(t)\cos\varphi\sin i(x)\cos a(x) \\
& + \cos\delta(t)\cos\varphi\cos i(x)\cos a(x) \\
& + \cos\delta(t)\cos h(t)\sin\varphi\sin i(x)\cos a(x) + \cos\delta(t)\sin h(t)\sin i_s\sin a(x)
\end{aligned} \qquad (1.9)$$

where φ is the latitude of the location defined positive for the northern hemisphere, $h(t)$ is the hour angle, $i(x)$ is the surface inclination defined as 0 for ceilings and $\pi/2$ for vertical walls, $a(x)$ is the surface azimuth defined as $-\pi/2$ if the surface outward normal points eastward and 0 if the normal points southward, and where $\delta(t)$ is the solar declination.

1.2.2 Shortwave radiation on a tilted surface

The total solar irradiation $E(t,x)$ on a arbitrary surface can be determined as the sum of the direct $E_D(t,x)$, diffuse $E_d(t,x)$ and reflected $E_r(t,x)$ radiation on the surface.

$$E(t,x) = E_D(t,x) + E_d(t,x) + E_r(t,x) \tag{1.10}$$

For a known profile of direct solar irradiation on a random surface, all three factors can be determined for another arbitrary surface s. Herefore, a profile of direct solar irradiation $E_{D,\perp}(t,x)$ perpendicular on the beam radiation is retrieved from Meteonorm and used as only input parameter. The calculation of other configurations besides normal to the solar beam is performed in the model.

Different models for the determination of the diffuse radiation do exist based on an isotropic or anisotropic model of the sky dome. On account of the high importance of solar irradiation for the model[1], a more detailed determination of diffuse radiation based on a anisotropic sky dome model is favorable. Herefore, the Perez model [16, 17] is implemented.

$$E_d(t,x) + E_r(t,x) = AE_{d,h}\left[0.5\left(1+\cos(i)\right)\left(1-F_1\right)+F_1\cos\xi(t,x)\cos^{-1}\xi_h(t)+F_2\sin(i)\right] \\ + 0.5\rho A\left(E_{D,h}+E_{d,h}\right)\left(1-\cos(i)\right) \tag{1.11}$$

wherefore A is the surface area, $E_{d,h}$ is the diffuse horizonal radiation, i is the surface inclination, F_1 is the circomsolar brightening coefficient, F_2, ρ is the ground reflectance and $E_{D,h}$ is the direct horizonal radiation. The brightening coefficients F_1, F_2 are determined as

$$F_n = F_{n,1}(\varepsilon) + F_{n,2}(\varepsilon)\Delta + F_{n,3}(\varepsilon)\xi_h(t) \tag{1.12}$$

where $F_{n,i}$ are determined in the Perez model [17] based on measurements, ε is the sky clearness and Δ is the sky brightness. Here, the sky brightness Δ is determined as $E_{d,h}E_{sc}^{-1}$ while the sky clearness ε is determined as

$$\varepsilon = \left(E_{d,h}+E_{D,h}\right)E_{d,h}^{-1} + \kappa\xi_h^3(t)\left(1+\kappa\xi_h^3(t)\right)^{-1} \tag{1.13}$$

wherefore E_{sc} is the solar constant and κ equals 1.041.

---

[1] Solar radiation interacts e.g. with the building thermal response, heat generation by means of a thermal solar collector and power generation with a photovoltaic array

Chapter 2
Transient building response model

Ruben Baetens and Dirk Saelens

Abstract A numeric building model is developed in Modelica for integrated energy simulation.

In this section, we describe in detail the dynamic building model and its possibilities that are implemented in Modelica as part of the IDEAS platform. The building model allows simulation of the energy demand for heating and cooling of a multi-zone building, energy flows in the building envelope and interconnection with dynamic models of thermal and electrical building energy systems within the IDEAS platform for comfort measures.

The description is divided into the description of the model and the model. The window model and the model for ground losses are described more in detail as extend to the wall model.

The relevant material properties of the surfaces are complex functions of the surface temperature, angle and wavelength for each participating surface. The assumptions used frequently in engineering applications [6] are that (*i*) each surface emits or reflects diffusely, that (*ii*) each surface is at a uniform temperature, that (*iii*) the energy flux leaving a surface is evenly distributed across the surface and (*iv*) is one-dimensional.

2.1 Wall response model

The description of the thermal response of a (or a structure of parallel opaque layers in general) is structured as in the 3 different occurring processes, i.e. the heat balance of the exterior surface, heat conduction between both surfaces and the heat balance of the interior surface.

Ruben Baetens
K.U.Leuven, Kasteelpark Arenberg 40 bus 2447, BE-3001 Leuven (Heverlee) e-mail: ruben.baetens@bwk.kuleuven.be

Dirk Saelens
K.U.Leuven, Kasteelpark Arenberg 40 bus 2447, BE-3001 Leuven (Heverlee) e-mail: dirk.saelens@bwk.kuleuven.be

2.1.1 Exterior surface heat balance

The heat balance of the exterior surface is determined as

$$Q_{net}(t,x) = Q_c(t,x) + Q_{SW}(t,x) + Q_{LW,e}(t,x) + Q_{LW,sky}(t,x) \tag{2.1}$$

where $Q_{net}(t,x)$ denotes the heat flow into the wall, $Q_c(t,x)$ denotes heat transfer by convection, $Q_{SW}(t,x)$ denotes short-wave absorption of direct and diffuse solar light, $Q_{LW,e}(t,x)$ denotes long-wave heat exchange with the environment and $Q_{LW,sky}(t,x)$ denotes long-wave heat exchange with the sky.

Convection. The exterior convective heat flow $Q_c(t,x)$ is computed as

$$Q_c(t,x) = 5.01 \, v_{10}(t)^{0.85} A(x) [T_{db}(t) - T_s(t,x)] \tag{2.2}$$

where $A(x)$ is the surface area, $T_{db(t)}$ is the dry-bulb exterior air temperature, $T_s(t,x)$ is the surface temperature and $v_{10}(t)$ is the wind speed in the undisturbed flow at 10 meter above the ground and where the stated correlation is valid for a v_{10} range of $[0.15, 7.5]$ meter per second [18]. The $v_{10}(t)$-dependent term denoting the exterior convective heat transfer coefficient $h_{ce}(t)$ is determined as $\max\{f(v_{10}), 5.6\}$ in order to take into account buoyancy effects at low wind speeds [19].

Longwave radiation. Longwave radiation between the surface and environment $Q_{LW,e}(x)$ is determined as

$$Q_{LW,e}(t,x) = \sigma \varepsilon_{LW}(x) A(x) \left[T_s(t,x)^4 - F_{sky}(x) T_{sky}(t)^4 - (1 - F_{sky}(x)) T_{db}(t)^4 \right] \tag{2.3}$$

as derived from the Stefan-Boltzmann law [20, 21] wherefore σ the Stefan-Boltzmann constant [22], $\varepsilon_{LW}(x)$ the longwave emissivity of the exterior surface, $A(x)$ is the surface area, $F_{sky}(x)$ the radiant-interchange configuration factor between the surface and sky [23] as defined on page 4, and the surface and the environment respectively and $T_s(t,x)$ and $T_{sky}(t)$ are the exterior surface and sky temperature respectively.

Shortwave radiation. Shortwave solar irradiation absorbed by the exterior surface $Q_{SW}(t,x)$ is determined as $\varepsilon_{SW}(x) A(x) E_S(t,x)$ where $\varepsilon_{SW}(x)$ is the shortwave absorption of the surface, $A(x)$ the surface area and $E_S(t,x)$ the total irradiation on the depicted surface. The calculation method for solar irradiation $E_S(t,x)$ depending on latitude, time, weather conditions, inclination and orientation is described in detail on page 4.

2.1.2 Wall conduction process

For the purpose of dynamic building simulation, the partial differential equation of the continuous time and space model of heat transport through a solid is most often simplified into ordinary differential equations with a finite number of parameters representing only one-dimensional heat transport through a construction layer. Within this context, the wall is mod-

eled with lumped elements, i.e. a model where temperatures and heat fluxes are determined from a system composed of a sequence of discrete resistances and capacitances R_{n+1}, C_n. The number of capacitive elements n used in modeling the transient thermal response of the denotes the order of the lumped capacitance model.

$$Q_{net}(t,w) = \frac{\partial T_c(t,w)}{\partial t}C(x) = \sum_{i}^{n} Q_{res,i}(t,x) + Q_{source}(t,x) \quad (2.4)$$

where $dQ_{net}(t,x)$ is the added energy to the lumped capacity, $T_c(t,x)$ is the temperature of the lumped capacity, $C_c(x)$ is the thermal capacity of the lumped capacity equal to $\rho(x)c(x,t)d_cA(x)$ for which $\rho(x)$ denotes the density and $c(x)$ is the specific heat capacity of the material, d_c the equivalent thickness of the lumped element and $A(x)$ the surface of the modeled layer, where $Q_{res}(t,x)$ the heat flux through the lumped resistance and $R_r(x)$ is the total thermal resistance of the lumped resistance equal to $d_r(\lambda(x,t)A(x))^{-1}$ for which d_r denotes the equivalent thickness of the lumped element and where Q_{source} are internal thermal source, e.g. from embedded systems.

Studies on the optimal order reduction for lumped construction elements in thermal building models can be found in literature [24, 25, 26, 27, 28], where optimization towards reduction is performed through comparison of zone air temperatures or comparison of Bode plots [29] on magnitude and phase for the low-order and a high-order lumped element. The general conclusion found towards model accuracy and computational efficiency depict that 1st-order lumped elements do not seem to be able to deal with radiation on the surfaces whereas 2nd-order lumped elements, i.e. based on two capacities and three resistances, give minimal loss of accuracy compared to high-order reference models for a limited computational effort. Both light and medium constructions [30] show high accuracy if a 2nd-order lumped element is used and little improvements can be achieved through optimization on nodal placement [24, 26, 27, 28] whereas a higher order thermal network should be used for heavy constructions [30] when the dynamics of the system are of concern as significant errors remain for simplified models at low frequency [27, 28, 31].

The model has a provision for including a temperature coefficient $f_{\lambda,c}$ to modify the thermal conductivity. The general description for the temperature dependency of the material thermal conductivity λ is $\lambda_0 + f_{\lambda,c}[T_C - T_0]$ where T_0 is the temperature for which the standard input thermal conductivity is defined at standard temperature and pressure (STP) conditions. If $f_{\lambda,c}$ is not defined, no temperature dependence is taken into account and set to unity.

2.1.3 Interior surface heat balance

The heat balance of the interior surface is determined as

$$Q_{net}(t,x) = Q_c(t,x) + \sum_{i}^{N} Q_{SW,i}(t,x) + \sum_{i}^{N} Q_{LW,i}(t,x) \quad (2.5)$$

where $Q_{net}(t,x)$ denotes the heat flow into the wall, $Q_c(t,x)$ denotes heat transfer by convection, $Q_{SW}(t,x)$ denotes short-wave absorption of direct and diffuse solar light netering the interior zone through windows and $Q_{LW,i}(t,x)$ denotes long-wave heat exchange with the surounding interior surfaces.

Convection. The surface heat resistances $R_s(t,x)$ for the exterior and interior surface respectively are determined as $R_s(t,x)^{-1} = A(x)h_c(t,x)$ where $A(x)$ is the surface area and where $h_c(t,x)$ is the exterior and interior convective heat transfer coefficient. The interior natural convective heat transfer coefficient $h_{ci}(t,x)$ is computed for each interior surface as

$$h_{ci}(t,x) = n_1(t,x)D(x)^{n_2(t,x)}|T_a(t,x) - T_s(t,x)|^{n_3(t,x)} \tag{2.6}$$

where $D(x)$ is the characteristic length of the surface, $T_a(t,x)$ is the indoor air temperature $T_s(t,x)$, and $n_i(t,x)$ are correlation coefficients. These parameters $\{n_1, n_2, n_3\}$ are identical to $\{1.823, -0.121, 0.293\}$ for vertical surfaces [32], $\{2.175, -0.076, 0.308\}$ for horizontal surfaces wherefore the heat flux is in the same direction as the buoyancy force [32], and $\{2.72, -, 0.13\}$ for horizontal surfaces wherefore the heat flux is in the opposite direction as the buoyancy force [33]. The interior natural convective heat transfer coefficient is only described as function of the temperature difference. An overview of a more detailed correlation including the possible higher wind velocities due to mechanical ventilation can be found in literature [34] but are not implemented.

Longwave radiation. Similar to the thermal model for heat transfer through a wall, a thermal circuit formulation for the direct radiant exchange between surfaces can be derived [35, 36, 37]. The resulting heat exchange by longwave radiation between two surface s_i and s_j can be described as

$$Q_{s_i,s_j}(t) = \sigma \left[\frac{1-\varepsilon_{s_i}}{\varepsilon_{s_i}} + \frac{1}{F_{s_i,s_j}} + \frac{A_{s_i}}{\sum_i A_{s_i}} \right]^{-1} A_{s_i} \left[T_{s_i}(t)^4 - T_{s_j}(t)^4 \right] \tag{2.7}$$

$$F_{s_i,s_j} = \int_{s_j} \cos\theta_p \cos\theta_s \pi^{-1} S_{s_i,s_j}^{-2} ds_j \tag{2.8}$$

as derived from the Stefan-Boltzmann law [20, 21] wherefore ε_{s_i} and ε_{s_j} are the emissivity of surfaces s_i and s_j respectively, F_{s_i,s_j} is radiant-interchange configuration factor [23] between surfaces s_i and s_j, A_{s_i} and A_{s_j} are the areas of surfaces s_i and s_j respectively, σ is the Stefan-Boltzmann constant [22] and T_{s_i} and T_{s_j} are the surface temperature of surfaces s_i and s_j respectively.

The above description of longwave radiation as mentioned above for a room or thermal zone results in the necessity of a very detailed input, i.e. the configuration between all needs to be described by their shape, position and orientation in order to define F_{s_i,s_j}, and difficulties to introduce windows and internal gains in the zone of interest. Simplification is achieved by means of a ΔY or *delta-star transformation* [38] and by definition of a (fictive) radiant star node in the zone model. Literature [39] shows that the overall model is not significantly sensitive to this assumption. The heat exchange by longwave radiation between surface s_i and the radiant star node in the zone model can be described as

$$Q_{s_i,rs}(t) = \sigma \left[\frac{1 - \varepsilon_{s_i}}{\varepsilon_{s_i}} + \frac{A_{s_i}}{\sum_i A_{s_i}} \right]^{-1} A_{s_i} \left[T_{s_i}(t)^4 - T_{rs}(t)^4 \right] \tag{2.9}$$

where ε_{s_i} is the emissivity of surface s_i, A_{s_i} is the area of surface s_i, $\sum_i A_{s_i}$ is the sum of areas for all surfaces s_i of the thermal zone, σ is the Stefan-Boltzmann constant [22] and T_{s_i} and T_{rs} are the temperatures of surfaces s_1 and the radiant star node respectively.

Shortwave radiation. Absorption of shortwave solar radiation on the interior surface is handled equally as for the outside surface. Determination of the receiving solar radiation on the interior surface after passing through windows is dealt with in the zone model.

2.1.4 Model extension for windows

The thermal model of a is similar to the model of an exterior wall but includes the absorption of solar irradiation by the different glass panes, the presence of gas gaps between different glass panes and the transmission of solar irradiation to the adjacent indoor zone.

Gap heat transfer. The total convective and longwave heat transfer through thin gas gaps as present in modern glazing systems is described as

$$\begin{aligned}
Q_{net}(t,x) = {} & A\lambda(x)d(x)^{-1}Nu(t,x)[T_{s_1}(t) - T_{s_2}(t)] \\
& + A\sigma\varepsilon_{s_1}\varepsilon_{s_2}[1 - (1 - \varepsilon_{s_1})(1 - \varepsilon_{s_2})]^{-1}\left[T_{s_1}^4(t) - T_{s_2}^4(t)\right]
\end{aligned} \tag{2.10}$$

where A is the glazing surface, $d(x)$ is the gap width, $Nu(t,x)$ is the Nusselt number of the gas, ε_{s_i} is the longwave emissivity of the surfaces and T_{s_i} is the surface temperature.

The Nusselt number of the present gas in the gap describing the ratio of convective to conductive heat transfer is generally described is

$$Nu(t,x) = n_1(t,x)Gr(t,x)^{n_2(t,x)} \tag{2.11}$$

$$Gr(t,x) = g\beta\rho^2 d(x)^3 \mu^{-2}[T_{s_1}(t) - T_{s_2}(t)] \tag{2.12}$$

where $Gr(t,x)$ is the Grashof number approximating the ratio of buoyancy to viscous force acting on the window gap gas, g is the gravitational acceleration, β is the coefficient of thermal expansion, ρ is the gas density, μ is the gas viscosity and $n_i(t,x)$ are correlation coefficients. These parameters $\{n_1, n_2\}$ are identical to $\{1.0, 0\}$ for all $Gr(t,x)$ below 7.10^3, $\{0.0384, 0.37\}$ for all $Gr(t,x)$ between 10^4 and 8.10^4, $\{0.41, 0.16\}$ for all $Gr(t,x)$ between 8.10^4 and 2.10^5 and $\{0.0317, 0.37\}$ for all $Gr(t,x)$ above 2.10^5.

Shortwave optical properties. The properties for absorption by and transmission through the glazing are taken into account depending on the angle of incidence of solar irradiation and are based on the output of the WINDOW 4.0 software [?, 40] as validated by Arasteh [41] and Furler [42]. Within this software, the angular dependence of the optical properties is determined based on the model of Furler [43]. The reflectivity r and transmissivity $t = 1 - r$ are determined with the Fresnel equations [44] and Snell's Law of refraction [45], based on the relative refractive index n as follows

$$r(t,x) = 0.5\sin^2\left(\xi(t,x) - \xi'(t,x)\right)\sin^{-2}\left(\xi(t,x) + \xi'(t,x)\right)$$
$$+ 0.5\tan^2\left(\xi(t,x) - \xi'(t,x)\right)\tan^{-2}\left(\xi(t,x) + \xi'(t,x)\right) \tag{2.13}$$

where $\sin\xi(t,x) = n\sin\xi'(t,x)$. The resulting transmittance $T(t,x)$ and reflectance $R(t,x)$ for a single glass pane after multiple reflections is obtained from

$$T(t,x) = t_0^2 e^{-\alpha(x)d(x)/\cos\xi(t,x)}\left[1 - r(t,x)^2 e^{-\alpha d(x)/\cos\xi(t,x)}\right]^{-1} \tag{2.14}$$

$$R(t,x) = r(t,x)\left[1 + T(t,x)e^{-\alpha(x)d(x)/\cos\xi(t,x)}\right] \tag{2.15}$$

where $d(x)$ is the thickness of the pane and $\alpha(x)$ is absorption coefficient. The total transmittance $T(t,x)$ and the absorptances $A_n(t,x)$ for multipane windows are retrieved using iterative equations taking into account the multiple internal reflections within the glazing system.

The resulting output from WINDOW 4.0 [?] depicts an array of the transmittances T through the window and the absorptances A_n for each glass pane n for $\xi_s \in \{(k/18)\}$ with $k \in \{0, 1, \ldots, 9\}$. The same array input is used in other dynamic building simulation tools, e.g. in TRNSYS [?] where values for different angles are retrieved by means of linear interpolation.

2.1.5 Model extension for ground slabs

The heat flow through building envelope constructions in contact with a is the same for the interior surface and the conduction process, but differs at the exterior surface in contact with the ground. As the heat transfer through the ground is 3-dimensional and defined by a large time lag, the exterior surface heat balance is generally approximated based on ISO 13370.

The total heat flow through the ground is given by

$$Q_{net}(t,x) = L_S(x)\left[\bar{T}_i - \bar{T}_e\right] - L_{pi}(x)\hat{T}_i\cos\gamma_i(t) + L_{pe}(x)\hat{T}_e\cos\gamma_e(t) \tag{2.16}$$

where L_S is the steady-state thermal coupling coefficient, L_{pi} and L_{pe} are the internal and external periodic thermal coupling coefficients respectively, $\bar{T}$ is the annual average temperature, $\hat{T}$ is the annual average temperature amplitude, and γ_i and γ_e determine the time lag of the heat flow cycle compared with that of the internal and external temperature respectively.

The steady-state and periodic thermal coupling coefficient area is determined as

$$L_S(x) = A(x)\frac{\lambda_g(x)}{0.457B_t(x) + d_t(x) + 0.5z} + zP(x)\frac{2\lambda_g}{\pi z}\left[1 + \frac{0.5d_t(x)}{d_t(x) + z}\right]\ln\left[\frac{z}{d_t} + 1\right] \tag{2.17}$$

$$L_{pi}(x) = A(x)\frac{\lambda_g(x)}{d_t(x)}\sqrt{\frac{2}{\left[1 + \frac{\delta}{d_t(x)}\right]^2 + 1}} \; ; \; L_{pe}(x) = 0.37P(x)\lambda_g(x)\ln\left[\frac{\delta}{d_t(x)} + 1\right] \tag{2.18}$$

where $A(x)$ is the wall area, λ_g is the thermal ocnductivity of the unfrozen ground, $B_t(x)$ is the characteristic dimension of the floor, $d_t(x)$ is the equivalent thickness of the wall construction, z is the depth of the wall (i.e. floor) below ground level, δ is periodic penetration depth (i.e. the depth in the ground at which the temperature amplitude is reduced to e^{-1} of that at the surface) and $P(x)$ is the exposed perimeter of the wall. The angle $\gamma_e(t)$ is determined as $2\pi t/t_{yr} + \pi/12 - \arctan d_t(x)/(d_t(x) + \delta)$ and $\gamma_e(t)$ is determined as $2\pi t/t_{yr} + \pi/12 + 0.22 \arctan \delta/(d_t(x) + 1)$.

2.2 Zone model

Consisting of both the convective as radiative calculation for determination of thermal comfort.

2.2.1 Thermal response model

Also the thermal response of a can be divided into a convective, longwave radiative and shortwave radiative process influencing both thermal comfort in the depicted zone as well as the response of adjacent wall structures.

Convective. The air within the zone is modeled based on the assumption that it is well-stirred, i.e. it is characterized by a single uniform air temperature. This is practically accomplished with the mixing caused by the air distribution system. The convective gains and the resulting change in air temperature T_a of a single thermal zone can be modeled as a thermal circuit. The resulting heat balance for the air node can be described as

$$
\frac{\partial T_a}{\partial t} c_a V_a = \sum_i^N Q_{i,a}(t) + \sum_i^{n_s} R_{s,ci}^{-1} A_{s,i} [T_a(t) - T_{s,i}(t)] + \sum_i^{n_z} \dot{m}_{a,z}(t) [h_a - h_{a,z}]
$$
$$
+ \dot{m}_{a,e} [h_a(t) - h_{a,e}(t)] + \dot{m}_{a,sys}(t) [h_a(t) - h_{a,sys}(t)] \tag{2.19}
$$

wherefore the specific air enthalpy h_a is determined as $c_a \vartheta_a + \chi_a c_w \vartheta_a + \chi_a h_{w,ev}$ and where T_a is the air temperature of the zone, c_a is the specific heat capacity of air at constant pressure, V_a is the zone air volume, Q_a is a convective internal load, $R_{s,i}$ is the convective surface resistance of surface s_i, $A_{s,i}$ is the area of surface s_i, $T_{s,i}$ the surface temperature of surface s_i, $\dot{m}_{a,z}$ is the mass flow rate between zones, $\dot{m}_{a,e}$ is the mass flow rate between the exterior by natural infiltration, $\dot{m}_{a,sys}$ is the mass flow rate provided by the ventilation system, ϑ_a is the air temperature in degrees Celsius, χ_a is the air humidity ratio, c_w is specific heat of water vapor at constant pressure and $h_{w,ev}$ is evaporation heat of water at 0 degrees Celsius.

Infiltration and ventilation systems provide air to the zones, undesirably or to meet heating or cooling loads. The thermal energy provided to the zone by this air change rate can be formulated from the difference between the supply air enthalpy and the enthalpy of the air leaving the zone h_a. It is assumed that the zone supply air mass flow rate is exactly equal to

the sum of the air flow rates leaving the zone, and all air streams exit the zone at the zone mean air temperature. The moisture dependence of the air enthalpy is neglected in most cases.

A multiplier for the zone capacitance $f_{c,a}$ is included. A $f_{c,a}$ equaling unity represents just the capacitance of the air volume in the specified zone. This multiplier can be greater than unity if the zone air capacitance needs to be increased for stability of the simulation. This multiplier increases the capacitance of the air volume by increasing the zone volume and can be done for numerical reasons or to account for the additional capacitances in the zone to see the effect on the dynamics of the simulation. This multiplier is constant throughout the simulation and is set to 5.0 if the value is not defined.

Longwave radiation. The exchange of longwave radiation in a zone has been previously described in Sect. 2.1.3 by Eq. 2.5 and further considering the heat balance of the interior surface. Here, an expression based on *radiant interchange configuration factors* of *view factors* is avoided based on a delta-star transformation and by definition of a *radiant star temperature* T_{rs}. Literature [39] shows that the overall model is not significantly sensitive to this assumption. This T_{rs} can be derived from the law of energy conservation in the radiant star node as $\sum_i Q_{s_i - rs}$ must equal zero. Long wave radiation from internal sources are dealt with by including them in the heat balance of the radiant star node resulting in a diffuse distribution of the radiative source[1].

Shortwave radiation. Transmitted shortwave solar radiation is distributed over all surfaces in the zone in a prescribed scale. This scale is an input value which may be dependent on the shape of the zone and the location of the windows, but literature [39] shows that the overall model is not significantly sensitive to this assumption.

2.2.2 Thermal comfort

For thermal measures, both the determination of an *operationally* or *dry resultant temperature* ϑ_c as well as the *predicted mean vote* (PMV) and *predicted percentage of dissatisfied* (PPD) are implemented.

Operationally temperature. A *dry resultant temperature* ϑ_c can be defined based on the previous assumptions for convective heat exchange, radiation and internal gains as

$$\vartheta_c(t) = \left[\vartheta_{mrt}(t) + \vartheta_a(t)\sqrt{10v_a(t)} \right] \left[1 + \sqrt{10v_a(t)} \right]^{-1} \tag{2.20}$$

which can be approximated by $0.5\left[\vartheta_{mrt} + \vartheta_a\right], \forall v_a \leq 0.1 m/s$ where ϑ_{mrt} and ϑ_a depict the mean radiative and air temperature respectively and v_a is the air velocity. Here, ϑ_{mrt} is determined as the area weighted surface temperature of the zone surfaces.

Comfort indicators. Most meaningful for expression the thermal environment is to state what percentage of persons can be expected to be decidedly dissatisfied. The *predicted percentage of dissatisfied* (PPD) [46] can be expressed as

---

[1] Note that, as a result, the radiant star temperature T_{rs} is not equal to the radiative temperature of the zone as will be perceived by occupants.

$$PPD = 100 - 95\ e^{-0.003353PMV^4 - 0.2179PMV^2} \tag{2.21}$$

as function the *predicted mean vote* (PMV) [47] which expresses the thermal person of persons in the commonly used psycho-physical ASHRAE scale between -3 and +3 [48]. The expression for PMV can be defined [46, 49] as

$$\begin{aligned} PMV = \Big[0.303\ e^{-0.036\ M_A} + 0.028\Big]\ \Big[&M_A - 3.96 \cdot 10^{-8} f_c\ \big[T_{cl}^4 - T_{mrt}^4\big] - f_{cl}h_c\ [T_{cl} - T_a] \\ &- 3.05\ [5.73 - 0.007\ M_A - p_{vp}] - 0.42\ [M_A - M_{eq}] - 0.0173\ M_A\ [5.87 - p_{vp}] \\ &- 0.0014\ M_A\ [34 - \vartheta_a]\Big] \end{aligned} \tag{2.22}$$

where M_A is the specific metabolic rate per body surface area of the human body, M_{eq} is the metabolic equivalent task equal to 58.15 Wm^{-2}, p_{vp} is the partial water vapor pressure, T_a is the air temperature, T_{cl} is the surface temperature of clothing, f_{cl} is the clothing area factor, T_{cl} is the mean radiant temperature and h_c is the convective heat transfer. The required clothing temperature T_{cl} can be determined as

$$T_{cl} = T_b - 0.0028\ M_A - R_{cl}\ \big[3.96\ 10^{-8} f_{cl}\ \big[T_{cl}^4 - T_{mrt}^4\big] + f_{cl}h_c\ [T_{cl} - T_a]\big] \tag{2.23}$$

where T_b is the body temperature equal to 308.95 K, R_{cl} depicts the thermal resistance from the skin to the outer surface of the clothed body and is equal to 0.155 I_{cl} where I_{cl} is teh so-called the *clo-value*, and where f_{cl} is determined as 1.05 $+ 0.1\ I_{cl}$ if $I_{cl} > 0.5$ or 1.00 $+ 0.2\ I_{cl}$ elsewhere.

Chapter 3
Thermal building system

Roel De Coninck and Lieve Helsen

Abstract A numeric thermal system model is developed in Modelica for integrated energy simulation.

Chapter 4
Electricity system

Juan Van Roy, Bart Verbruggen and Johan Driesen

Abstract A numeric electric system model is developed in Modelica for integrated energy simulation.

In this section, we describe in detail the electrical models that are implemented in Modelica as part of the IDEAS platform. These are models on the production, electrical distribution and storage side. First the photovoltaic (PV) system is treated which produces electricity locally from solar energy. In a second part, the distribution of electricity on distribution level is described.

Work in progress are the in-home electricity grid and the electrical storage in batteries.

4.1 Photovoltaic system

First, a photovoltaic (PV) system is implemented based on the five parameter model to simulate the energy production from a photovoltaic system under operational conditions. The five parameter model, which is temperature dependent, is based on the single diode equivalent circuit of a PV panel [50, 51]. The five parameters are:

- the light current, I_{ph};
- the diode reverse saturation current, I_o;
- a shunt resistance, R_{sh};
- a series resistance, R_s;
- the thermal voltage, V_t.

These parameters are indicated in the equivalent circuit presented in Figure 4.1.

Bart Verbruggen

K.U.Leuven, Kasteelpark Arenberg 10 bus 2445, BE-3001 Leuven (Heverlee) e-mail: `bart.verbruggen@esat.kuleuven.be`

Juan Van Roy

K.U.Leuven, Kasteelpark Arenberg 10 bus 2445, BE-3001 Leuven (Heverlee) e-mail: `juan.vanroy@esat.kuleuven.be`
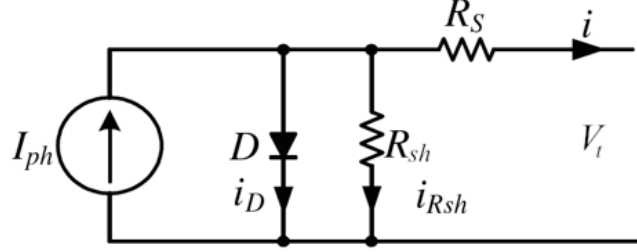
Fig. 4.1 Five parameter model of a PV panel [50]

4.1.1 Power output of PV panel

The electrical output from a PV system depends on the solar radiation, the ambient temperature of the cells, the solar incidence angle and the load. The solar radiation, incidence angle and temperature is obtained from chapter **??**. The parameters needed for the model can generally be obtained from data gathered from the manufacturer's specifications of the solar panels. The required specifications to calculate the five parameters are the current I_{mpp} and voltage V_{mpp} at maximum power point (mpp) under standard testing conditions (STC)[1], the short circuit current I_{sc} and open circuit voltage V_{oc} under the same standard testing conditions, the temperature coefficients k_i and k_v of respectively the short circuit current and open circuit voltage and the nominal cell temperature under STC $T_{c,ref}$.

The general current-voltage $(i - v)$ equation for the single diode equivalent circuit is given in Eq. (4.1). This equation can be written for three points: (i) short-circuit, (ii) open-circuit and (iii) maximum power point [51].

$$i(t) = I_{ph} - I_0 \left(e^{\frac{v(t)+i(t)R_S}{n_s V_t}} - 1 \right) - \frac{v(t)+i(t)R_s}{R_{sh}} \tag{4.1}$$

In this equation V_t is the junction thermal voltage and n_s the number of cells in the panel connected in series:

$$V_t = \frac{f_A k T_{stc}}{q} \tag{4.2}$$

with f_A the ideality factor, k the Boltzmann's constant ($1.380663 \cdot 10^{-23}$ J/K), q the charge of an electron ($1.600218 \cdot 10^{-19}$ C) and T_{stc} the cell temperature under STC.

The voltage V_{mpp} and current I_{mpp} at maximum power point should satisfy Eq. (4.1). The derivative of the power with respect to the voltage (dP/dV) at V_{mpp} and I_{mpp} should be zero Eq. (4.3). The derivative of the current with respect to the voltage (dI/dV) at short circuit current should be the negative of the shunt conductance (R_{sh}^{-1}). These equations lead to the calculation of the parameters R_s, R_{sh} and V_t.

The maximum power point P_{mpp} (at $I = I_{mpp}$) can be found with Eq. (4.3):

---

[1] Standard testing conditions are (i) an irradiance of 1000 W/m^2 and (ii) a cell temperature of 25°C and (iii) reference air mass of 1.5

$$\frac{dP}{dV} = I_{mpp} + V_{mpp} \frac{-\frac{(I_{sc}R_{sh}-V_{oc}+I_{sc}R_s)e^{\frac{V_{mpp}+I_{mpp}R_s-V_{oc}}{n_sV_t}}}{n_sV_tR_{sh}} - \frac{1}{R_{sh}}}{1 + \frac{(I_{sc}R_{sh}-V_{oc}+I_{sc}R_s)e^{\frac{V_{mpp}+I_{mpp}R_s-V_{oc}}{n_sV_t}}}{n_sV_tR_{sh}} + \frac{R_s}{R_{sh}}} \tag{4.3}$$

The reverse saturation current I_o and light current I_{ph} at STC can be found based on Eq. (4.1) for the short circuit (Eq. (4.4)) and open circuit condition (Eq. (4.5)).

$$I_{sc} = I_{ph} - I_0 e^{\frac{I_{sc}R_s}{n_sV_t}} - \frac{I_{sc}R_s}{R_{sh}} \tag{4.4}$$

$$I_{oc} = 0 = I_{ph} - I_0 e^{\frac{V_{oc}}{n_sV_t}} - \frac{V_{oc}}{R_{sh}} \tag{4.5}$$

The PV parameters are adjusted to take into account the position of the sun, the direct and indirect radiation and the ambient temperature. The cell temperature has been adjusted to be the ambient temperature plus the losses of the panel. The parameters for the non-reference conditions are calculated in the next paragraphs.

The tilt angle and orientation of the PV panels are parameters of the PV model. Together with the sun's position, the incidence angle of the direct beam radiation can be calculated which allows to obtain the amount of radiation that gets reflected by and passes through the PV panel cover. This is done using incidence angle modifiers that are derived from De Soto et al. [50]. The incidence angle modifier $K_{\tau\alpha}(\theta)$ can be found from the transmittance τ of the cover system with Eq. (4.8), which is approximated in Eq. (4.7). The angle of refraction, θ_r, is determined in Eq. (4.6) by Snell's law, with θ the incidence angle and n the effective index of refraction of the cell cover. In Eq. (4.7), f_K is the glazing extinction coefficient and f_L is the glazing thickness. In the model f_K and f_L can be adjusted. By default, f_K is assumed to be 4 m^{-1} and f_L is assumed to be 2 mm.

$$\theta_r = \arcsin(n\sin\theta) \tag{4.6}$$

$$\tau(\theta) = e^{-\frac{f_Kf_L}{\cos\theta_r}}\left[1 - \frac{1}{2}\left(\frac{\sin^2(\theta_r-\theta)}{\sin^2(\theta_r+\theta)} + \frac{\tan^2(\theta_r-\theta)}{\tan^2(\theta_r+\theta)}\right)\right] \tag{4.7}$$

$$K_{\tau\alpha}(\theta) = \frac{\tau(\theta)}{\tau(0)} \tag{4.8}$$

The incidence angle modifiers and the direct and diffuse radiation, which are inputs to the model, allow together with the reflected radiation to calculate the absorbed solar radiation S in Eq. (4.9). In this equation G_b is the direct, G_d the diffuse and G the total radiation. The slope of the PV panel is characterized by β.

$$\frac{S}{S_{ref}} = \frac{G_b}{G_{ref}}K_{\tau\alpha,b} + \frac{G_d}{G_{ref}}K_{\tau\alpha,d}\frac{1+\cos\beta}{2} + \frac{G}{G_{ref}}\rho K_{\tau\alpha,g}\frac{1-\cos\beta}{2} \tag{4.9}$$

with

$$S_{ref} = G_{ref}e^{-f_Kf_L} \tag{4.10}$$

and G_{ref} is the irradiance at STC (1000 W/m^2).

The light current I_{ph}, reverse saturation current I_0 and thermal voltage V_t at non-reference conditions can be calculated when the temperature, open circuit voltage and short circuit current are known [51]. The open circuit voltage V_{oc} can be calculated using Eqns. (4.11) and (4.12). The short circuit current I_{sc} can be found using Eq. (4.13).

$$e^{\frac{V_{oc}(S)}{n_s V_t}} = \frac{I_{ph}(S)R_{sh} - V_{oc}(S)}{I_0 R_{sh}} \tag{4.11}$$

$$V_{oc}(T) = V_{oc} + k_v(T - T_{stc}) \tag{4.12}$$

$$I_{sc}(S,T) = I_{sc}\left(\frac{S}{S_{ref}}\right)\left(1 + \frac{k_i}{100}(T - T_{ref})\right) \tag{4.13}$$

The reverse saturation current I_0 can be calculated with Eq. (4.14). The light current I_{ph} is found using Eq. (4.15).

$$I_0 = \left(I_{sc} - \frac{V_{oc} - I_{sc}R_s}{R_{sh}}\right)e^{-\frac{V_{oc}}{n_s V_t}} \tag{4.14}$$

$$I_{ph} = I_0 e^{\frac{V_{oc}}{n_s V_t}} + \frac{V_{oc}}{R_{sh}} \tag{4.15}$$

4.1.2 Power output of PV system

A PV system consists of multiple PV panels connected in series. Assuming that all PV panels are in the same condition, the output DC voltage can be multiplied by the number of PV panels in a PV system.

The number of PV panels is a parameter of the general PV system model. The peak power P_{peak} is defined with V_{mpp}, I_{mpp} and the number of panels n_p:

$$P_{peak} = n_p V_{mpp} I_{mpp} \tag{4.16}$$

4.1.3 Orientation PV system

The PV system has two orientation parameters, namely (i) the azimuth and (ii) the inclination angle. An azimuth angle of $0°$ is defined as towards the South, $-90°$ for the East and $90°$ for the West. Applied to Belgium, the PV system has the highest annual electricity production when the system is oriented directly to the South with an inclination of $34°$.

The inclination and azimuth angles are paremeters of the modeled photovoltaic system.

4.1.4 Inverter

A PV system is connected to the electrical grid through an inverter, which converts the generated DC power to AC power with an efficiency $\eta_{dc/ac}$.

Due to the lack of simultaneity of production and consumption, a bidirectional energy flow may occur between a building and the electrical grid (e.g. low voltage grid for residential buildings), which may lead to voltage instabilities on the grid (e.g. increasing voltages due to the injection of electricity, unbalance, etc.). To avoid excessive feeder voltages at the moments of re-injecting PV power in the grid, the inverter is curtailed when a predefined voltage limit is reached. Curtailing of a PV system means production losses.

4.2 Electrical distribution grid

In the electrical grid system two types of grids exist, namely (*i*) distribution and (*ii*) transmission grids [52, 53]. However, in Belgium, distribution grids differ fundamentally from transmission grids:

- They are mostly radially: This means there is only one feeding transformer[2]. Due to the lack of a redundant supply, the reduced reliability is a major disadvantage. In case of a fault, all loads behind the fault will be switched off.
- The lower the voltage level, the higher the R/X ratio. Thus, low voltage residential distribution grids are highly resistive.

An electrical distribution grid for low voltage is modeled. E.g. a residential district is typically a radial distribution grid with a rated nominal voltage of 230/400 V[3] wye (or star) connection. Both a single-phase en three-phase grid can be simulated. The single-phase grid can serve for fully balanced simulations.

First, the grid topology is described. As will be shown, any radial grid can be easily represented by two matrices, namely the incidence and impedance matrix. Second, the background for the power flow analysis will be described to determine the nodal currents, line currents and nodal voltages. Radial grids are, compared to meshed grids, more easy to analyze and because of the low cost, it is prefered for distribution grids [52]. Figure 4.2 gives an example of a radial grid. This figure shows an IEEE 34 node test feeder [54].

4.2.1 Grid topology

Distribution grids for low-voltage are mostly radial grids. In this case, a residential three-phase distribution grid is modeled. A residential district is typically a radial feeder with a rated nominal voltage of 230/400V wye (or star) connection. For distribution grids without

---

[2] Traditionally, there is only a unidirectional power flow.

[3] 230 V phase voltage, 400 V line voltage.

Fig. 4.2 Grid topology IEEE 34 node test feeder [54]

distributed generation (uni-directional power flow), the voltage at the feeder typically has a higher value to ensure that the voltage in the whole feeder stays within the preset boundaries. For a fully balanced system, the single-phase equivalent grid can be used. Connections to loads (e.g. buildings) are represented by nodes. Loads and generation units can be single or three-phase connected to the grid.

Any radial grid can be represented by an incidence matrix (or connection matrix) **T**. The columns correspond with the number of nodes. Each line in **T** represents a segment of the grid (branch) between two nodes. Each segment is represented by 1 and -1 at respectively the start and end node of that segment. The other row elements are zero. A node can be the start or end node of more than one segment. Since there are n nodes, a radial grid consists of $n-1$ line segments. To attain a square matrix, an additional (first) row is introduced to represent the imaginary line segment between the transformer and the first node. This line segment only has an end node.

Eq. (4.17) gives an example of the representation of an incidence matrix **T** in which the nodes are all next to each other, which means branches are between consecutive nodes.

$$\mathbf{T} = \begin{bmatrix} -1 & 0 & 0 & \cdots & 0 & 0 & 0 \\ 1 & -1 & 0 & \cdots & 0 & 0 & 0 \\ 0 & 1 & -1 & \cdots & 0 & 0 & 0 \\ \vdots & \vdots & \vdots & \ddots & \vdots & \vdots & \vdots \\ 0 & 0 & 0 & \cdots & -1 & 0 & 0 \\ 0 & 0 & 0 & \cdots & 1 & -1 & 0 \\ 0 & 0 & 0 & \cdots & 0 & 1 & -1 \end{bmatrix} \tag{4.17}$$

Cables, with a length f_L (m), for the line segments of an electrical grid are characterized by an impedance $Z = R + jX$, with R the resistance and X the reactance of the cable:

$$R = f_L r \tag{4.18}$$

$$X = f_L x \tag{4.19}$$

with r the characteristic resistance x the characteristic reactance in Ω/m. This allows to represent the grid with an impedance matrix $\mathbf{Z} = \mathbf{R} + j\mathbf{X}$.

In a similar way, the houseconnectors are described. These are the connection lines between the in-home grid and the grid connection node of the building. The houseconnec-

tors are characterized by a cable type, cable length and the type of connection with the grid (single-phase or three-phase connection).

4.2.2 Power flow analysis

A power flow analysis is required to characterize the impact of a load profile on each connection node in the grid. A power flow analysis is performed to determine the nodal currents $\mathbf{I}_{node}$, line currents $\mathbf{I}_{line}$ and nodal voltages $\mathbf{V}_{node}$. The calculations are based on the Laws of Kirchhoff:

Conservation of electric charge At any node, the sum of currents flowing into the node is equal to the sum of currents flowing out of the node (Eq. (4.20)).

Conservation of energy The sum of the voltage drops around any closed circuit is zero (Eq. (4.21)).

$$\sum_{k=1}^{nodes} i_k(t) = 0 \tag{4.20}$$

$$\sum_{k=1}^{branches} \Delta v_k(t) = 0 \tag{4.21}$$

The voltage drop in a branch k between nodes n and $n+1$ is defined as:

$$\Delta v_k(t) = Z_k i_{line,k}(t) = v_n(t) - v_{n+1}(t). \tag{4.22}$$

When the nodal currents $\mathbf{I}_{node}$, line currents $\mathbf{I}_{line}$ and nodal voltages $\mathbf{V}_{node}$ are known, the total flow of apparent power S can be calculated. S consists of active power P and reactive power Q:

$$S(t) = \sum_{f=1}^{phases} P_f(t) + jQ_f(t) \tag{4.23}$$

The apparent power S is calculated as:

$$S = U_{phase} I^* \tag{4.24}$$

with U_{phase} the phase voltage and I^* the complex conjugate of I.

The ohmic losses in a single-phase grid are calculated as follows:

$$P_{grid\ loss,\ 1-phase} = \sum_{k=1}^{branches} P_{k,\ loss} = \sum_{k=1}^{branches} R_k I_{k,\ line}^2 \tag{4.25}$$

A three-phase distribution grid consists of three phases and a neutral cable. Therefore, Eq. (4.25) can be rewritten for three-phase distribution grids as follows:

$$P_{grid\ loss,\ 3-phase} = \sum_{f=1}^{phases} P_{grid\ loss,\ f} + P_{neutral,\ loss} \qquad (4.26)$$

4.2.3 Single/three-phase grid simulation

Electrical loads, generation units, storage units (e.g. batteries) can be single-phase or three-phase connected to the grid. Generally the system is not fully balanced (e.g. the same load in each phase for each node in the distribution grid) and an unbalanced three-phase power flow analysis is performed. In case of a fully balanced system, the power flow analysis can be performed on a simplified single-phase grid. For three-phase power flows, the distribution grid is represented by three phase conductors and a neutral conductor. Nodal phase voltages are the voltages with respect to the nodal voltage in the neutral conductor.

4.2.4 Transformer

A radial distribution grid has one feeding transformer. The low-voltage (LV) side of the transformer is connected to the distribution grid, while the high-voltage (HV) side is connected to the higher-voltage grid.

A transformator (single or three-phase) is represented by the equivalent scheme as shown in Figure 4.3. The transformer is represented by series ($Z_{s,HV}$ and $Z_{s,LV}$) and parallel element (Z_{par}). The series impedances represent the ohmic resistance and reactance (inductance) of respectively the high-voltage and low-voltage windings of the transformer. The parallel impedance represents the magnetic losses (or iron losses) in the core of the transformer. To define the active losses of the transformer, only the resistances of all impedances are taken into account.
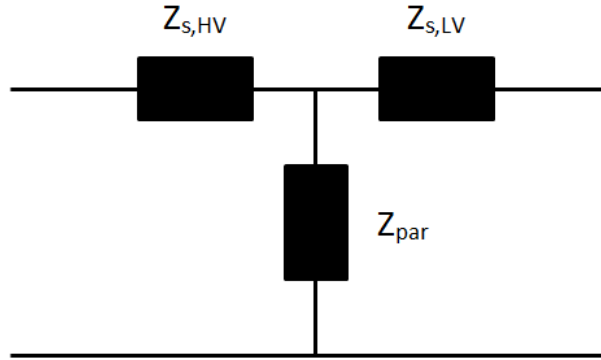

Fig. 4.3 Equivalent scheme of a transformator

The parallel element (Z_{par}) is defined during a no-load test of the transformer. At the primary side, the nominal voltage is applied, while the secondary windings are open. The series elements can be neglected:

$$Z_{par} = \left[\frac{400}{\sqrt{3}}\right]^2 \left[\frac{P_0}{3}\right]^{-1} \tag{4.27}$$

with P_0 the no-load losses.

The series elements ($Z_{s,HV}$ and $Z_{s,LV}$) are defined during short-circuit tests of the transformer. During this test, the secondary windings are shorted. Since the parallel elements are large compared to the series elements, the series elements ($Z_s = Z_{s,HV} + Z_{s,LV}$) can be defined:

$$Z_s = \left[\frac{400u_k}{100\sqrt{3}}\right]^2 \left[\frac{S_n u_k}{300}\right]^{-1} \tag{4.28}$$

with S_n the nominal apparent power of the transformer and u_k the percentage of the short-circuit voltage[4]. Generally, Z_s is evenly distributed amongst $Z_{s,HV}$ and $Z_{s,LV}$.

The active losses in a transformer are calculated as is done in Eq. (4.25) for the losses in the grid.

4.3 Electrical in-home grid

In progress.

4.4 Electrical storage

In progress.

---

[4] The short-circuit voltage is the voltage that has to be applied at the primary winding to have the nominal current in the primary winding when the secondary winding is shorted.

Part II
Validation or verification

val-i-dation (n.) 1. To declare or make legally valid. 2. To mark with an indication of official sanction. 3. To establish the soundness of; corroborate.

Chapter 5
Building energy simulation test - BESTEST

Ruben Baetens and Dirk Saelens

5.1 Introduction

The thermal building model are *validated* by comparative tests based on the *Building Energy Simulation Test* (BESTEST) [55, 56] as developed under supervision of the International Energy Agency (IEA) [57, 58] and standardized as the ANSI/ASHRAE Standard 140-2007 [59]. This standard consists of a series of specified test cases and has been developed to diagnose whole building energy simulation software. Here, output values such as the annual energy consumptions, peak loads, average and extreme room air temperatures, and some hourly data are compared to miscellaneous building energy simulation programs, e.g. BLAST, DOE2.1D, ESP-R, SERIRES / SUNCODE, S3PAS, TASE and TRNSYS.

5.1.1 Building energy simulation test cases

Within this work, the so-called *basic test cases* are used to *validate* the building model. These test cases test the ability to model combined effects as thermal mass, solar gains and solar shading, air infiltration, internal heat gains, sunspaces and thermostat control. Three series of basic cases are tested :

1. Qualification cases 600 to 650 representing a set of lightweight buildings that are relatively realistic with respect to their thermal characteristics. Within this set of cases, case 600 tests the south solar transmission, case 620 tests the east and west solar transmittance and incidence, case 640 tests night setback and case 650 tests venting.

––––––––––––––––––––

Ruben Baetens

K.U.Leuven, Kasteelpark Arenberg 40 bus 2447, BE-3001 Leuven (Heverlee) e-mail: ruben.baetens@bwk.kuleuven.be

Dirk Saelens

K.U.Leuven, Kasteelpark Arenberg 40 bus 2447, BE-3001 Leuven (Heverlee) e-mail: dirk.saelens@bwk.kuleuven.be

2. Qualification cases 900 to 960 representing a set of heavyweight buildings that are relatively realistic with respect to their thermal caracteristics and include a building configuration with a sunspace. Within this set of cases, case 900 tests the thermal mass and solar interaction, test 920 tests the east and west transmittance and its mass interaction, case 940 tests night set-back and its mass interaction, case 950 tests venting and its mass interaction and case 960 tests passive solar and interzonal heat transfer.
3. Free-float basic test cases 600FF, 900FF, 650FF and 950FF equaling the corresponding non-FF cases except the absence of a mechanical heating or cooling systems.
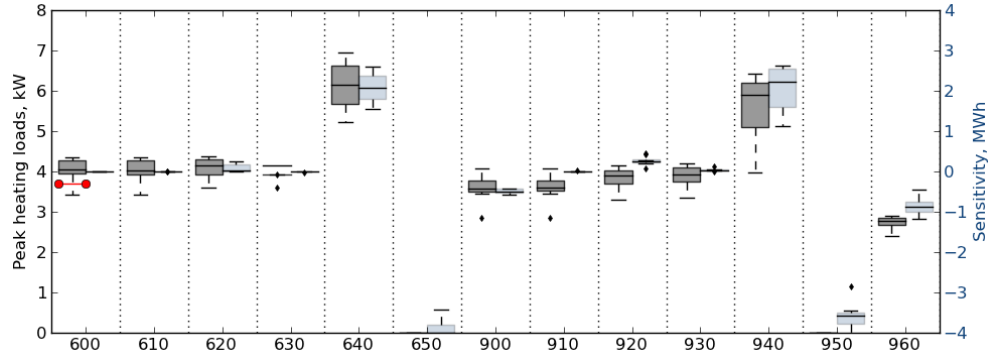
5.1.2 Test results

5.1.2.1 Annual heating and cooling loads

(a) Annual heating loads for the low mass and heavy mass buildings.

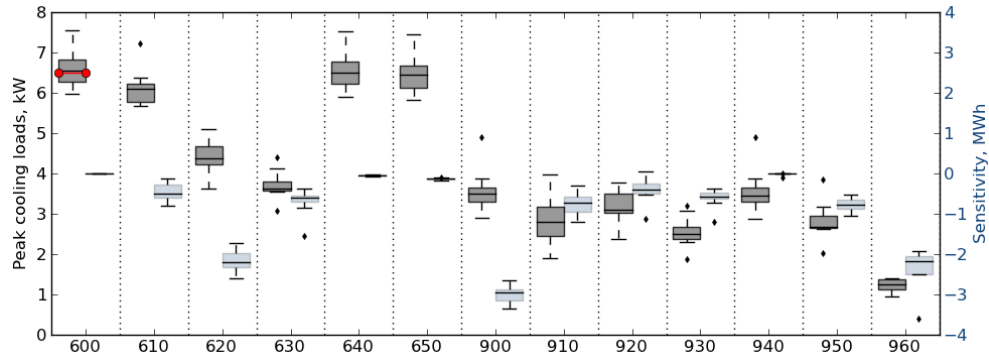(b) Annual sensible cooling loads for the low mass and heavy mass buildings.

Fig. 5.1 Annual heating and sensible cooling loads for the low mass and heavy mass buildings.
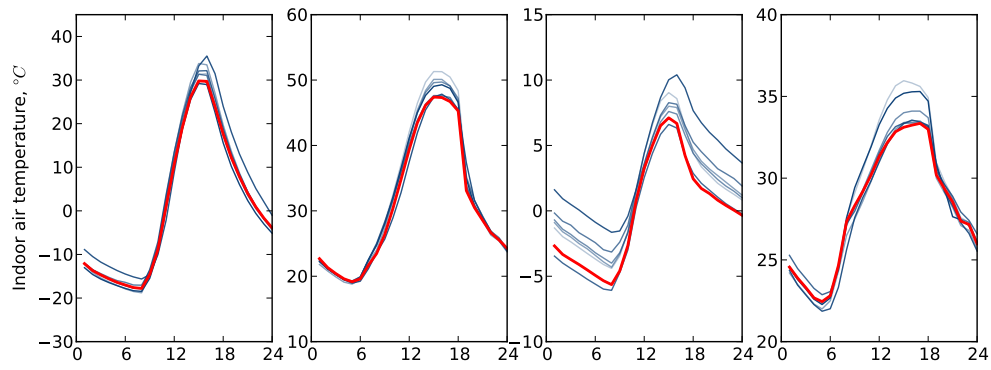
5.1.2.2 Peak heating and cooling loads

(a) Peak heating loads for the low mass and heavy mass buildings.

(b) Peak sensible cooling loads for the low mass and heavy mass buildings.

Fig. 5.2 Peak heating and sensible cooling loads for the low mass and heavy mass buildings.

5.1.2.3 Indoor air temperatures

Fig. 5.3 Indoor temperatures for the low mass and heavy mass buildings.

Chapter 6
Thermal building energy system test - BESTEST

Roel De Coninck and Lieve Helsen

Abstract A numeric thermal system model is developed in Modelica for integrated energy simulation.

Chapter 7
IEEE Distribution system analysis for radial test feeders

Juan Van Roy, Bart Verbruggen and Johan Driesen

Abstract A numeric electric system model is developed in Modelica for integrated energy simulation.

Part III
Bibliography

bibliography (n.) 1. A list of the works of a specific author or publisher. 2. a. A list of writings relating to a given subject: a bibliography of Latin American history. b. A list of writings used or considered by an author in preparing a particular work. 3. a. The description and identification of the editions, dates of issue, authorship, and typography of books or other written material. b. A compilation of such information.

References

1. Meteotest, "METEONORM Version 6.1 - Edition 2009," 2008.

2. National Climatic Data Center (NCDC), *Typical Meteorological Year User's Manual TD-9734, Hourly Solar Radiation - Surface Meteorological Observations*. Asheville: National Climatic Data Center, U.S. Department of Commerce, 1981.

3. European Commission, *Test Reference Years, Weather data sets for computer simulations of solar energy systems and energy consumption in buildings, CEC DG XII*. Brussels: European Comission, 1985.

4. National Climatic Data Center (NCDC), *Test reference year (TRY) DSI-9706*. Asheville: National Climatic Data Center, U.S. Department of Commerce, 1976.

5. ASHRAE, *Weather year for energy calculations*. Atlanta: : American Society of Heating, Refrigerating and Air-Conditioning Engineers, Inc., 1985.

6. G. N. Walton, *Thermal analysis research program reference manual*. Washington: U.S. Department of Commerce, National Bureau of Standards, 1983.

7. M. Martin and P. Berdahl, "Characteristics of infrared sky radiation in the United States," *Solar Energy*, vol. 33, pp. 321–336, 1984.

8. P. Berdahl and F. Fromberg, "The thermal radiance of clear skies," *Solar Energy*, vol. 29, pp. 299–314, 1982.

9. P. Berdahl and M. Martin, "Emissivity of clear skies," *Solar Energy*, vol. 32, pp. 663–664, 1984.

10. F. Kasten and G. Czeplak, "Solar and terrestrial radiation dependent on the amount and type of cloud," *Solar Energy*, vol. 24, pp. 177–189, 1979.

11. M. Perraudeau, "Daylight availbility from energetic data," in *CIE Daylighting conference Vol.I*, (Moscow), p. A17, 1990.

12. R. H. van Gent, "on the History of Astronomy," 2011.

13. J. W. Spencer, "Fourier series representation of the position of the sun," *Search*, vol. 2, no. 5, p. 172, 1971.

14. J. A. Duffie and W. A. Beckman, *Solar engineering of thermal processes*. New York: John Wiley & Sons Inc, first ed ed., 1980.

15. M. Iqbal, *An introduction to solar radiation*. New York - London: Academic Press Inc, 1983.

16. R. Perez, R. Stewart, C. Arbogast, R. Seals, and J. Scott, "An isotropic hourly diffuse radiation model for sloping surfaces: Description, performance validation, site dependecy evaluation," *Solar Energy*, vol. 36, no. 6, pp. 481–497, 1986.

17. R. Perez, R. Seals, P. Ineichen, R. Stewart, and D. Meniucci, "A new simplified version of the Perez diffuse irradiance model for tilted surfaces," *Solar Energy*, vol. 39, no. 3, pp. 221–231, 1987.

18. T. Defraeye, B. Blocken, and J. Carmeliet, "Convective heat transfer coefficient for exterior building surfaces: Existing correlations and CFD modelling," *Energy Conversion and Management*, vol. 52, no. 1, pp. 512–522, 2011.

19. W. Jürges, "Der Wärmeübergang an einer ebenen Wand," *Beihefte zum Gesundheits-Ingenieur*, vol. 1, no. 19, 1924.

20. J. Stefan, "Über die Beziehung zwischen der Wärmestrahlung und der Temperatur," *Sitzungsberichte der mathematisch-naturwissenschaftlichen Classe der kaiserlichen Akademie der Wissenschaften*, vol. 79, pp. 391–428, 1879.

21. L. Boltzmann, "Ableitung des Stefan'schen Gesetzes, betreffend die Abhängigkeit der Wärmestrahlung von der Temperatur aus der electromagnetischen Lichttheorie," *Annalen der Physik und Chemie*, vol. 22, pp. 291–294, 1884.

22. P. J. Mohr, B. N. Taylor, and D. B. Newell, "CODATA Recommended values of the fundamental physical constants: 2006," *Reviews of Modern Physics*, vol. 80, pp. 633–730, 2008.

23. D. C. Hamilton and W. R. Morgan, "Radiant-interchange configuration factors," tech. rep., National Advisory Comittee for Aeronautics, Washington, 1952.

24. A. Tindale, "Thrird-order lumped-parameter simulation method," *Building Services Engineering Research & Technology*, vol. 14, no. 3, pp. 87–97, 1993.

25. M. M. Gouda, S. Danaher, and C. P. Underwood, "Low-order model for the simulation of a building and its heating system," *Building Services Engineering Research & Technology*, vol. 21, pp. 199–208, 2000.

26. M. Gouda, "Building thermal model reduction using nonlinear constrained optimization," *Building and Environment*, vol. 37, pp. 1255–1265, Dec. 2002.

27. S. Wang and X. Xu, "Simplified building model for transient thermal performance estimation using GA-based parameter identification," *International Journal of Thermal Sciences*, vol. 45, pp. 419–432, 2006.

28. X. Xu and S. Wang, "Optimal simplified thermal models of building envelope based on frequency domain regression using genetic algorithm," *Energy and Buildings*, vol. 39, pp. 525–536, 2007.

29. H. W. Bode, *Network analysis and feedback amplifier design*. New York: Van Nostrand Co., 1945.

30. ASHRAE, *2009 ASHRAE Handbook: fundamentals*. Atlanta: ASHRAE American Society of Heating Refrigerating and Air-Conditioning Engineers, 2009.

31. G. Masy, *Definition and validation of a simplified multizone dynamic building model connected to heating system and HVAC unit*. Phd, Université de Liège, 2008.

32. A. J. N. Khalifa, "Ntural convective heat transfer coefficient - a review : Surfaces in two- and three-dimensional enclosures," *Energy Conversion and Management*, vol. 42, no. 4, pp. 505–517, 2001.

33. H. B. Awbi and A. Hatton, "Natural convection from heated room surfaces," *Energy and Buildings*, vol. 30, no. 3, pp. 233–244, 1999.

34. I. Beausoleil-Morrison, *The adaptive coupling of heat and air flow modeling within dynamic whole-building simulation*. PhD thesis, 2000.

35. H. Buchberg, *Electric analogue prediction of thermal behavior of an inhabitable enclosure*. Msc, University of California, 1954.

36. H. Buchberg, "Electric analogue prediction of thermal behavior of an inhabitable enclosure," *ASHRAE Transactions*, vol. 61, pp. 339–386, 1955.

37. A. K. Oppenheim, "Radiation analysis by the network method," *Transactions of American society of mechanical engineers*, vol. 78, pp. 725–735, 1956.

38. A. E. Kenelly, "Equivalence of triangles and stars in conducting networks," *Electrical World and Engineer*, vol. 34, pp. 413–414, 1899.

39. R. J. Liesen and C. O. Pedersen, "An evaluation of inside surface heat balance models for cooling load calculations," *ASHRAE Transactions*, vol. 103 Part 2, pp. 485–502, 1997.

40. E. U. Finlayson, D. K. Arasteh, C. Huizenga, M. D. Rubin, and M. S. Reilly, "WINDOW 4.0: Documentation of calculation procedures," tech. rep., 1993.

41. D. K. Arasteh, J. Hartmann, and M. Rubin, "Experimental verification of a model of heat transfer through windows," *ASHRAE Transactions*, vol. 93, no. 1, pp. 1425–1431, 1986.

42. R. A. Furler, P. Williams, and F. K. Kneubühl, "Experimental and theoretical studies on the energy balance of windows - NEFF Project report 177.1," tech. rep., 1988.

43. R. A. Furler, "Angular dependence of optical properties of homogeneous glasses," *ASHRAE Transactions*, vol. 97, no. 2, 1991.

44. M. A. Fresnel, "Mémoire sur la diffraction de la lumière," *Mémoires de l'Académie des Sciences (Paris)*, vol. 5, pp. 33–475, 1926.

45. V. Snellius, *Doctrina triangulorum*. 1627.

46. ISO 7730, *Ergonomics of the thermal environment - Analytical determination and interpretation of themal comfort using calculation of the PMV and PPD indices and local thermal comfort criteria*. Aug. 2005.

47. P. O. Fanger, *Thermal comfort: Analysis and application in environmental engineering*. New York: McGraw-Hill Book Company, 1970.

48. ANSI/ASRAE Standard 55-2004, *Thermal environmental conditions for human occupancy*. 2004.

49. ASHRAE, *ASHRAE Handbook - Fundamentals (SI Edition)*. 2009.

50. W. De Soto, S. Klein, and W. Beckman, "Improvement and Validation of a Model for Photovoltaic Array Performance," *Solar Energy*, vol. 80, pp. 78–88, 2006.

51. D. Sera, R. Teodorescu, and P. Rodriguez, "PV panel model based on datasheet values," in *IEEE International Symposium on Industrial Electronics*, pp. 2392–2396, 2007.

52. E. Haesen, *Multi-Objective Optimization of the Integration of Stochastic Distributed Energy Resources in Electricity Grids*. PhD thesis, 2009.

53. H. Willis, *Power Distribution Planning Reference Book*. 2004.

54. W. Kersting, "Radial Distribution Test Feeders," in *IEEE Power Engineering Society Winter Meeting*, (Columbus, Ohio), pp. 908–912, 2001.

55. R. Judkoff and J. Neymark, "International energy agency building energy simulation test (BESTEST) and diagnostic method," tech. rep., National Renewable Energy Laboratory, U.S. Department of Energy, Colorado, 1995.

56. J. Neymark and R. Judkoff, "International energy agency building energy simulation test and diagnostic method (IEA BESTEST) - In-depth diagnostic cases for ground coupled heat transfer related to slab-on-grad construction," tech. rep., National Renewable Energy Laboratory, U.S. Department of Energy, Colorado, 2008.

57. K. J. Lomas, H. Eppel, C. Martin, and D. Bloomfield, "Empirical validation of thermal building simulation programs using test room data - Volume 1: Final report," in *IEA Energy Conservation in Buildings and Community Systems Programme Annex 21 & IEA Solar Heating and Cooling Programme Task 12*, 1994.

58. K. J. Lomas, H. Eppel, C. Martin, and D. Bloomfield, "Empirical validation of thermal building simulation programs using test room data - Volume 2: Empircial validation package," in *IEA Energy Conservation in Buildings and Community Systems Programme Annex 21 & IEA Solar Heating and Cooling Programme Task 12*, 1994.

59. ASHRAE, *ANSI/ASHRAE Standard 140-2001 - Standard method of test for the evaluation of building energy analysis computer programs*, vol. 8400. American Society of Heating, Refrigerating and Air Conditioning Engineers, 2004.

Index